Int J Adv Manuf Technol (2014) 74:151–161
DOI 10.1007/s00170-014-5980-7

ORIGINAL ARTICLE

Mechanistic force modeling and machinability evaluation on MR-compatible materials

Shan Jiang · Zhaowei Ren · Zhengxing Wu

Received: 6 July 2013 / Accepted: 18 May 2014 / Published online: 29 May 2014
© Springer-Verlag London 2014

Abstract Magnetic resonance imaging (MRI)-guided surgical robots are becoming a hotspot owing to the good quality of MR image and stability of robot. For the MR-compatible robot, machinability influences assembly accuracy and kinematic accuracy directly. At the same time, the cutting force plays a vital role in evaluating machinability and machining process. This paper presents the machinability evaluation on five kinds of MR-compatible materials and an improved mechanistic force model. The model takes shearing and edge forces of flank and bottom edge combined with tool runout into consideration. Experimental results show that the prediction error is within 9 %. The effects that chip shape imposes on the machining stability and surface roughness are analyzed and then involved in the machinability evaluation. Digraph and matrix method are applied to evaluate the material machinability based on cutting force, roughness, and the chip shape. Relative importance between the three components is analyzed and taken into the evaluation. At last, polyformaldehyde is proved to have the best machinability.

Keywords MR-compatible robot · Cutting force · Chip shape · Surface roughness · Machinability

1 Introduction

Accurate brachytherapy of radioactive seed implantation involving the use of a robotically steered system has been of great interest of many researchers, especially in the last decades [1]. Magnetic resonance imaging (MRI) has a high resolution and precise geometry in soft tissues imaging. Therefore, robots based on MRI-guidance combining the advantages of minimally invasive surgery are drawing more and more attention [2, 3]. The common standard mechanical parts of a surgical robot cannot be used in MR environment [4–6] because they usually contain ferromagnetic components and will affect the MR images. Therefore, the robot should be manufactured with non-ferromagnetic materials, i.e., MR-compatible materials. On the other hand, MR-compatible materials' processing quality, which is mainly determined by machinability, influences the robot assembly accuracy and kinematic accuracy seriously.

Many kinds of parameters can be used to evaluate materials' machinability, such as cutting force, surface roughness, and chip shape. Similarly, multiple methods could be applied to evaluate machinability. Cutting force is one of the crucial components of machinability evaluation and an important index to evaluate the difficulty of machining, as it affects the quality and the precision of the products. Thus, it is essential to build a reliable quantitative model of milling forces for improving machining performance. It is also important for further prediction of the machine tool vibrations, necessary power, and processing stability.

Typically, there are four different approaches to build cutting force models: direct mapping method, numerical simulation model method, the prediction model method based on the feed drive or spindle motor current, and mechanistic model method [7]. The direct mapping method can build the mechanistic model by a large quantity of data [8], as a result, a large number of experiments must be done. Numerical methods are used to study the tool tip zone and interaction between the tool and the workpiece [9]. The most widely used numerical method is the finite element method (FEM). It could be applied in metal cutting simulation, considering material model, tool-chip interaction, and thermal-mechanical coupling [10]. However, the high calculation cost of its intrinsic interpolation procedure results in severe restrictions. For example,

S. Jiang (✉) · Z. Ren · Z. Wu
School of mechanical engineering, Tianjin University,
300072 Tianjin, China
e-mail: shanjmri@tju.edu.cn

the finite element method requires many assumptions and parameters in the models which are difficult to estimate. Models based on the feed drive or spindle motor current primarily relies on the mechanical feed drive system or the spindle structure, so noise may be included in the predicted results. Mechanistic methods that use a series of relations between process variables and cutting forces (or energy) assume that the cutting forces are proportional to the cross-sectional area of the uncut chip [11–13]. Mechanistic process models consider that the cutting forces acting on the tool edge is the function of the chip area and cutting force coefficients, which are calibrated from machining tests. A comprehensive review of mechanistic force models has been presented by Ehmann et al. [14]. Gonzalo et al. [15] proposed that cutting force coefficients depend on the tool–material couple, cutting conditions, and geometry of the tool. Roth et al. [16] presented a mechanistic model of the milling process based on an adaptive and local depth buffer of the computer graphics card compared to a traditional simulation method. Engin et al. [17] presented generalized mathematical models of solid end mills. Edouard and Enrico [18] improved an identification algorithm for the modeling of radial runout effect on the undeformed chip thickness. The previous models are based on the tools with zero degree helix angles for convenience, and they always neglect the tool runout effect and the bottom edge forces. This paper presents an improved mechanistic force model which overcomes the problems of previous studies. Experimental results show the model fits the experiment data well.

Many methodologies can be implemented to evaluate machinability of material, such as fuzzy comprehensive evaluation [19], data envelopment analysis [20], diagraph and matrix [21, 22], machining database [23], radar chart [24], etc. For fuzzy comprehensive evaluation, it is inevitable that subjectivity will affect the results. Data envelopment analysis is a method to evaluate the relative efficiency of a set of decision-making units (DMUs) in a production process. Data envelopment analysis models provide efficiency scores that assess the performance of the different DMUs in terms of either the use of several inputs or the production of certain outputs, but *interaction between the DMUs* is not considered. Machining database methodology is based on the database of metals' properties and used to evaluate the machinability. In another word, plenty of time and mass of data are needed to establish the database. Radar chart is used to determine the rank of merits of the materials qualitatively, compared with the typical radar chart, which is affected by subjectivity very likely. Unlike the foregoing methods, the factors used in diagraph and matrix method are normalized to integers on a scale from 0 to 10 and relative importance of the factors is involved. Machinability evaluation result could be obtained by calculating machinability matrix. Owing to the good efficiency, the diagraph and matrix method are applied in this paper.

Due to the importance of the machinability, this paper evaluates the machinability of the candidate materials based on three components: cutting force, roughness, and the chip shape. Considering the importance of cutting force in machinability evaluation and machining process, this paper presents an improved theoretical mechanistic cutting force model, considering the effect of undeformed chip thickness, runout angle, and friction, which will be illustrated in Section 2. The machinability of specific materials which are selected for manufacturing the MR-compatible robot is analyzed by using the diagraph and matrix method, and this part is given in Section 3. The main contributions of this work are concluded in Section 4.

2 Mechanistic force modeling

2.1 Mechanistic force modeling for flat-end milling

The schematic of flat-end milling is shown in Fig. 1a. Due to the existence of bottom and flank rubbing or ploughing effects, there are two separate mechanisms leading to forces in flat-end milling: shearing with chip formation and rubbing without chip formation. Cutting pressures loaded on the flank edge have different magnitudes and directions according to the cutting edge position. In Fig. 1a, both the helical and bottom edges engage in the cutting process, so contributions of shearing and rubbing on the flank and bottom edges are involved in the calculation of the total cutting force.

Figure 1b shows the cutting force acting on point P on a tooth of a cutting edge, which is perpendicular to the cutter axis. The cutting force acting on the helical flute rake face is dependent on the undeformed chip thickness. Given the uncut chip thickness, h, for each engaged cutting flute element, the differential cutting force is computed. It can be seen from Fig. 1a, c that bottom edges engage in the cutting process, while the material is cut by the flank edge. As the end of the tool is flat, the cutting effect caused by bottom edges is shown in Fig. 1c by the line-connecting points A and B. The total cutting force calculation acting on the flank edges is as following: firstly, cutter is divided into a finite number of axial disk elements of equivalent axial length, then differential force of each tooth on a slice is calculated, and thirdly, the total cutting force is obtained by differential force integration. The forces generated by bottom edges can be expressed in a linear function of chip width. The differential force components induced by chip removal and rubbing effects acting on the i th helical edge of j th axial disk element can be expressed as a linear superposition [25]:

$$\begin{cases} dF_{t,i,j}(h) = dF_{tc}(h) + dF_{te}(h) \\ dF_{r,i,j}(h) = dF_{rc}(h) + dF_{re}(h) \end{cases} \quad (1)$$

where $dF_{t,i,j}(h)$ and $dF_{r,i,j}(h)$ are the differential force in tangential and radial direction, respectively. $dF_{qc}(h)$ $(q=t,r)$ is the

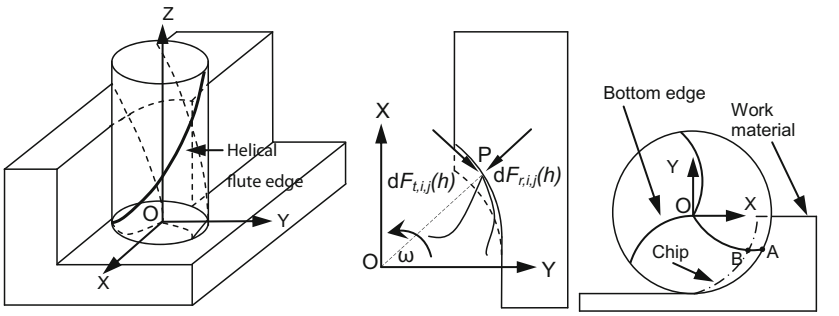

(a) Cutting procedure (b) Forces generated on flank edges (c) Forces generated on bottom edges

Fig. 1 Schematic of cutting mechanism of end milling of three-flute cutter

differential shearing force while $dF_{qe}(h)(q=t,r)$ is the differential rubbing force. $dF_{qc}(h)$ and $dF_{qe}(h)$ have the following form:

$$\begin{cases} dF_{qc}(h) = K_{qc} h_{i,j}(\psi_{i,j}) dz \\ dF_{qe}(h) = K_{qe} dz \end{cases} \qquad q = t or r \tag{2}$$

where K_{qc} is the shearing coefficient, K_{qe} is the edge coefficient, dz is the chip width in each of the discrete element cutting edge, and $h_{i,j}(\psi_{i,j})$ is the undeformed chip thickness.

The positioning angle $\psi_{i,j}$ of each element of the cutting edge is determined by

$$\begin{cases} \psi_{i,j} = \eta_{i,j} + \theta + \theta_p \\ \eta_{i,j} = a_p j / n / \tan\beta \end{cases} \tag{3}$$

where $\eta_{i,j}$ is helix lag angle, θ is the spindle rotation angle, $\theta=\omega t$ where ω indicates the angular velocity, $\theta_p=2(i-1)\pi/n$ is the pitch angle for a cutter with n uniformly spaced teeth, and β is the helix angle.

From the equations above, the calculation of uncut chip thickness and the tooth-positioning angle is important for determining the differential cutting force. Calculation of the uncut chip thickness and tooth position is based on the flute paths. Unlike other mechanical machining processes, milling is affected by many variables, which make its process and modeling very complicated. Usually, trajectory of tool edge is defined by tool radius, spindle angular velocity, tool runout effect, and feed rate. Among these characteristics, tool runout is an important aspect of research within modeling, simulation, and control of milling forces [26]. Tool radial runout is a common problem in the milling process mainly caused by poor rigidity of the system or the tool-workpiece and so on [27]. The principal form of runout is the cutting tool center offset as shown in Fig. 2, where point O is the geometry center of the tool and point O' is the center of the tool holder. The runout offset, e, indicates the deviation from the cutter axis to the tool holder axis.

Due to radial runout, the chip thickness calculation should be modified according to the real edge trajectory, instead of the traditional computational method which states that thickness at tooth entrance and exit near the normal direction are 0 [15]. The influence of eccentricity on chip thickness of the related slice can be modified by the following equation [28]:

$$h_{i,j}(\psi_{i,j}) = f_z \sin(\psi_{i,j}) + \begin{bmatrix} \sin(\psi_{i,j}+\gamma) \\ \cos(\psi_{i,j}+\gamma) \end{bmatrix}^T \begin{bmatrix} e\sin(\psi_0+\gamma) \\ e\cos(\psi_0+\gamma) \end{bmatrix} \tag{4}$$

where f_z denotes the feed per tooth, e denotes the runout offset, $\psi_{i,j}$ denotes the location angle which is defined at the bottom section of the cutter and measured anticlockwise from the offset direction to a given tooth tip, ψ_0 is the eccentricity angle, and γ is the initial position of the tool.

A control function is defined as the following to check whether the flank edges engage in cutting or not.

$$g(\psi_{i,j}) = \begin{cases} 1 & \psi_s \le \psi_{i,j} \bmod 2\pi \le \psi_e \,\&\, h_{i,j} \ge 0 \\ 0 & else \end{cases} \tag{5}$$

here, ψ_s and ψ_e are the locations of the start and end points of contact of the cutting edge.

In order to calculate the total force applied on the whole flute edge, the differential forces are resolved into the feed (x)

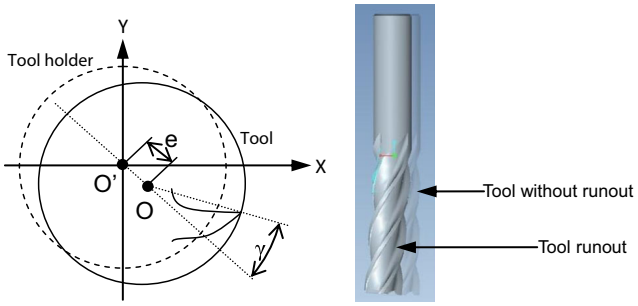

(a) Schematic of tool runout (b) 3D model of tool runout

Fig. 2 Tool runout

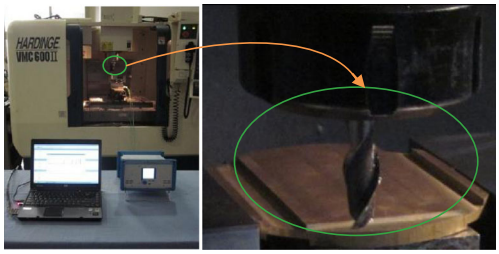

(a) Experimental setup (b) Cutting tool

Fig. 3 Experimental setup and the cutting tool

and normal (y) directions. Thus, total cutting force can then be obtained in the following way:

$$\begin{bmatrix} F_x \\ F_y \end{bmatrix} = g_i(\psi_{i,j}) \sum_{i=1}^{n} \sum_{j=1}^{m} \begin{bmatrix} -\cos\psi_{i,j} & \sin\psi_{i,j} \\ -\sin\psi_{i,j} & -\cos\psi_{i,j} \end{bmatrix} \begin{bmatrix} F_t \\ F_r \end{bmatrix} \quad (6)$$

where $g_i(\psi_{i,j})$ is the control function defined to check whether the flank edges engage in cutting. The tangential and radial forces are treated as a linear function of the chip area and the cutting edge length. F_t and F_r are [25]

$$\begin{bmatrix} dF_t \\ dF_r \end{bmatrix} = \begin{bmatrix} K_{tc} h_{i,j}(\psi_{i,j}) dz + K_{te} dS \\ K_{rc} h_{i,j}(\psi_{i,j}) dz + K_{re} dS \end{bmatrix} \quad (7)$$

K_{qc} and $K_{qe}(q=t,r)$ represent cutting force and edge force coefficients, respectively. Both of them are considered as constants [25]; in other words, they are independent of cutting parameters. dS denotes the length of the discrete cutting edge element which can be substituted by dz for convenience. According to the geometry of the tool, the following equation can be obtained.

$$r d\psi = \tan\beta dz \quad (8)$$

Rewritten Eq. (8) as

$$d\psi = \tan\beta dz / r \quad (9)$$

where r is the cutter radius. So, integration of axial height can be transformed to angular position.

As the edge-rubbing mechanism can be modeled as a linear function of axial depth of cut [29] while the bottom edge cutting process is similar to the rubbing process; thus, the bottom edge-induced cutting forces can be treated as a linear function of the length of the contact line AB, which is defined as the bottom uncut chip width. The forces induced by the bottom edges can also be portrayed by tangential, radial, and axial (not present in this study) components as follows:

$$\begin{cases} dF_{b,t,i,j}(\psi_{i,j}) = dF_{b,t}(\psi_{i,j}) \\ dF_{b,r,i,j}(\psi_{i,j}) = dF_{b,r}(\psi_{i,j}) \end{cases} \quad (10)$$

where $F_{b,t,i,j}(\psi_{i,j})$ and $F_{b,r,i,j}(\psi_{i,j})$ are the bottom edge-induced cutting forces acting on the helical edge i of axial disk j from the tangential and radial direction, respectively. $F_{b,t}(\psi_{i,j})$ and $F_{b,r}(\psi_{i,j})$ are the bottom edge-induced cutting forces from the tangential and radial direction, respectively.

$$\begin{cases} dF_{b,t}(\psi_{i,j}) = K_{b,t}(\psi_{i,j}) db \\ dF_{b,r}(\psi_{i,j}) = K_{b,r}(\psi_{i,j}) db \end{cases} \quad (11)$$

where $K_{b,t}$ and $K_{b,r}$ denote the tangential and radial coefficients, respectively; db denotes the width of the undeformed chip which approximates to the line AB and $h_{i,1}(\psi_{i,1})$.

Summing up the cutting forces acting on the n helical flutes of m slices and the forces generated by the bottom edges gives the total force applied on the cutter:

$$\begin{bmatrix} F_x \\ F_y \end{bmatrix} = g_i(\psi_{i,j}) r / \tan\beta \sum_{i=1}^{n} \left\{ \sum_{j=1}^{m} \int_{\psi_s}^{\psi_e} \begin{bmatrix} -\cos\psi_{i,j} & \sin\psi_{i,j} \\ -\sin\psi_{i,j} & -\cos\psi_{i,j} \end{bmatrix} \begin{bmatrix} K_{tc} h_{i,j}(\psi_{i,j}) + K_{te} \\ K_{rc} h_{i,j}(\psi_{i,j}) + K_{re} \end{bmatrix} d\psi_{i,j} + \begin{bmatrix} F_{b,t} \\ F_{b,r} \end{bmatrix} \right\} \quad (12)$$

2.2 Milling experiments and model validation

The cutting force experiment is shown in Fig. 3. Slot milling experiment was conducted on a 25-kW HARDINGE VMC-600II vertical machining center with maximum 12,000 rpm rotational speed. The workpiece material is Brass H59 with the hardness of HV130. The physical and mechanical properties of the material are given in Table 1.

The cutting forces during milling experiments were measured by a Kistler 9257A dynamometer and Kistler 5070 charge amplifier. The sensitivity of the dynamometer along x, y, and z directions are 7.901, 7.942, and 3.707 pc/N, respectively. Milling forces in x, y, and z directions were recorded

Table 1 Physical and mechanical properties of Brass H59

Density (g/cm3)	Young' modulus (GPa)	Tensile strength (MPa)	Elongation (%)
8.39	105	410	3

Table 2 Cutting conditions

Test number	Rotational speed (rpm)	Feed (mm/tooth)	Axial depth of cut (mm)
1	640	0.0375	1.5
2	640	0.0455	1.5
3	640	0.0375	2
4	640	0.0455	2
5	960	0.0455	1.5
6	960	0.0375	2

with a sampling rate of 1,024 Hz. Measurements were repeated three times to check the consistency of the measurements. The *x*-axis of the dynamometer is aligned with feed direction of the milling tool. The cylindrical end milling tool (SWT HSS-AL) used in slotting experiments has two teeth with 35° helix angle as shown in Fig. 3b. Considering size effect, feed per tooth and axial depth of cut cannot be too small. The range of experimental test cases chosen for this study is shown in Table 2.

Cutting forces in tests 1, 2, 3, and 4 are shown in Fig. 4a–d. The cutting force coefficients are identified by solving the inverse problem presented in Eq. (12) applying a least squares fitting method. The identification can be done using all the experimental values or selected intervals such as the interval containing the peak values. In this study, the values of the intervals involving the peak values are adopted. Cutting force and edge force coefficients are shown in Table 3. Coefficients of aluminum, nylon, polyformaldehyde, and polypropylene are also identified according to the method described above and listed in Table 3.

The suitability of the proposed force model is assessed according to the experimental and calculation results of the proposed model. Numerical simulations based on the cutting parameters of tests 5 and 6 are done and shown in Fig. 5a–d.

Comparing these results to the measured cutting forces, it is found that there is a good fitness. Although cutting parameters, such as spindle speed, feed per tooth, and depth of cut, are different, the model match experimental ones well in shape, frequency, and magnitude, and the remaining deviations are slight and negligible. Due to noisy signals such as uncertain factors of the piezoelectric dynamometer or the tiny foundation vibrations in the experimental environment, perturbations of measured cutting forces exist. Even in this condition, the trends of simulation and experimental data are in good agreement, and the average deviation is within 9 %. The result demonstrates that the modified model is valuable for machining process prediction, quality control, and reducing economy cost.

3 Machinability evaluation

Two kinds of metals and three kinds of engineering plastics, which have been validated in MR environment, are chosen to do the machinability test. For different materials with different

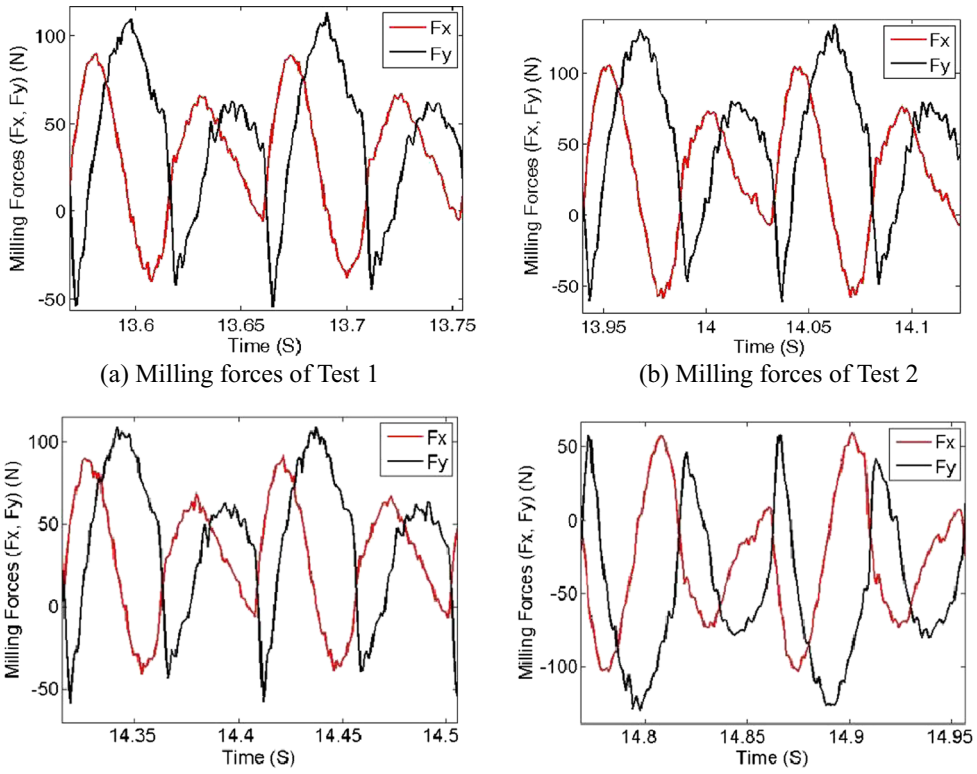

(a) Milling forces of Test 1

(b) Milling forces of Test 2

(c) Milling forces of Test 3

(d) Milling forces of Test 4

Fig. 4 Cutting force measurements of brass

Table 3 Cutting force and edge force coefficients

	K_{tc}	K_{rc}	K_{te}	K_{re}	$K_{b,te}$	$K_{b,re}$
Brass	572.3	246.6	19.5	9.7	405.2	206.4
Aluminum	472.0	229.3	18.3	9.0	377.5	192.3
Nylon	129.7	57.1	4.3	1.9	79.7	40.6
Polyformaldehyde	107.4	48.8	3.9	1.8	74.1	37.7
Polypropylene	65.1	32.9	2.9	1.3	52.9	26.9

material properties, the optimal processing parameters or tool-workpiece combination are supposed to be different. The materials are the candidates for manufacturing the MR robot; thus, it is more practical to process the materials under the same cutting parameters and compare their performance [21]. The differences of experimental results of the materials are obvious, and it is easy to make the choice.

3.1 Materials

The materials used in this study and their properties are listed in Table 4. It can be seen from the table that materials' properties are different from each other, but they all fulfill the requirement of strength or hardness of the MR-compatible robot.

3.2 Machinability components tests

1. Cutting force test: milling tests were conducted under the same conditions as described in Section 2.2. Each material was cut under the four groups of parameters as shown in Table 5.
2. Chip shape identification: chip shape of different material was detected during the milling process.
3. Surface roughness measurement: surface roughness (Ra) was measured by Taylor–Hobson TALYSURF 120 roughmeter; Fig. 6 shows the measurement process. Sampling length is 3 mm with 8,000 measured sampling points per millimeter. Ra was measured three times at the first, middle, and end region surface of the groove, respectively, with the speed 0.25 mm/s.

3.3 Results and discussion

Cutting force of the five kinds of materials in test 1 are shown in Fig. 7a–e. It can be seen that cutting force along x and y directions are varying periodically. The machined materials show different characteristics owing to different properties. The resultant forces of average forces of x and y directions are shown in Fig. 7f.

It can be seen from the broken lines that cutting forces of the five kinds of materials vary in the same trend under the parameters of the four groups. Cutting force of brass is the maximum, while polypropylene (PP) is the minimum which means PP is the easiest to be machined and consumes the least energy.

Two kinds of chips were formed during the milling process, as shown in Fig. 8. The first type is the short and curly chips, which are like the letter "C," produced by Aluminum 6061

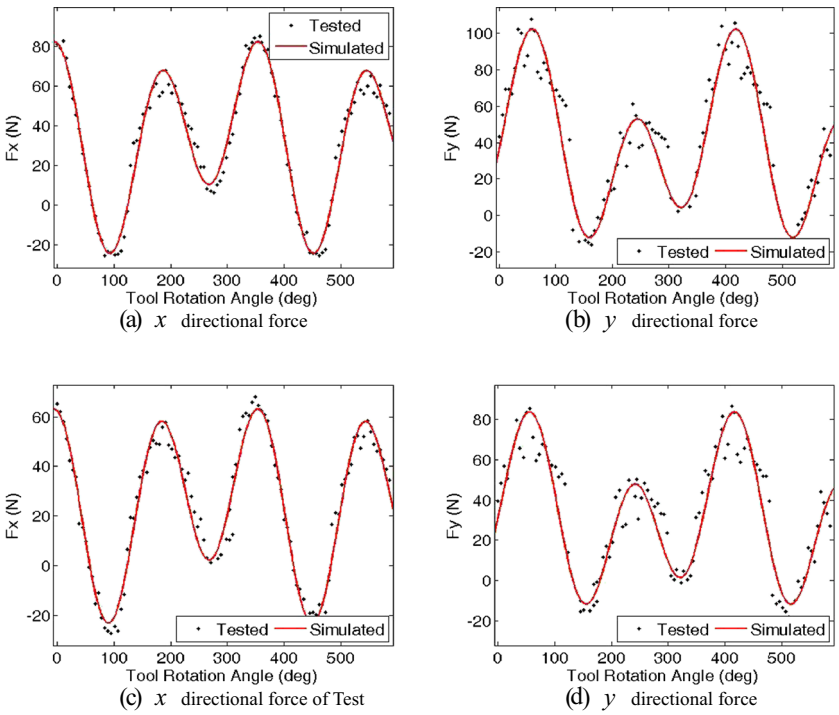

Fig. 5 Comparison of simulations and the experimental results: **a**, **b** test 5 and **c**, **d** test 6

Table 4 Materials' properties

Material	Density (g/cm^3)	Tensile strength (MPa)	Hardness
Brass H59	8.39	410	HV130
Aluminum 6061	2.8	265	HV95
Polyformaldehyde (POM)	1.39	63	M90
Nylon	1.15	60	M110
Polypropylene (PP)	0.9	20	RHN82.6

and PP. The second type is the long, tight, and curly chips produced by brass, nylon, and polyformaldehyde (POM). The former would not wind on the tool or the workpiece. On the contrary, it may collide with the tool's flank face or the workpiece surface. Then, the continuous frequent collision and fracture would affect the machining stability. Thus, the machining process of Brass H59, nylon, and POM is more smooth than that of polypropylene.

Surface roughness: surface topographies of test 1 are presented in Fig. 9a–e. As materials compositions are different, surface roughness profiles obtained under the same test show different characteristics. Variation of surface roughness values Ra in four tests are given in Fig. 9f.

It can be seen that as feed per tooth increases, surface becomes rougher. This is because successive marks become more separated and more cutting marks leave on the workpiece's surface [30]. Also, the trend lines indicate that the surface roughness values decrease when cutting speed is increased. It means that the lower the cutting force, the lower the vibration. It can be seen that polypropylene surface is coarser than the other materials. The results demonstrate that machined surface is smoother if the speed is controlled in a specific range with low feed rate.

3.4 Machinability evaluation

A lot of factors can be used to evaluate the machinability of a specific material. Machinability factors can be divided into beneficial attributes and non-beneficial attributes. A beneficial attribute (e.g., material removal rate) means the greater the attribute values, the better the machining performance, whereas a non-beneficial attribute (e.g., energy consumed)

Table 5 Milling parameters

Test number	Rotational speed (rpm)	Feed (mm/tooth)	Axial depth of cut (mm)
1	640	0.0375	1.5
2	640	0.0455	2
3	960	0.0375	2
4	960	0.0455	1.5

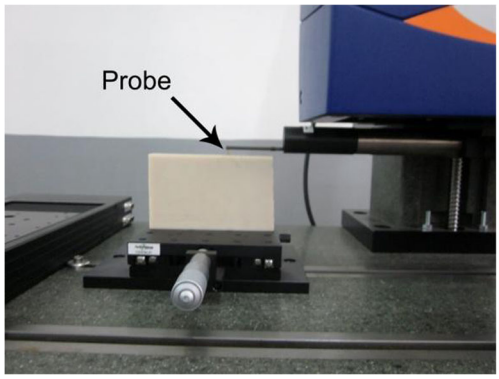

Fig. 6 Surface roughness measurement

possesses the opposite meaning. Here, the attributes used in the evaluation (cutting force, chip shape, and surface roughness) are all non-beneficial attributes. The quantitative values have different units; therefore, it is desirable to convert the quantitative values on the same scale between 0 and 10 for the convenience of calculating. The formula of transformation of non-beneficial attributes is given in Eq. (13) [21].

$$\begin{aligned} A_{ii} &= 10 \;/\; (1-A_i/A_{i\max}) \;\times\; A_i \quad A_{i\min}=0 \\ A_{ii} &= [10/(A_{i\max}-A_{i\min})] \times (A_{i\max}-A_i) \quad A_{i\min} > 0 \end{aligned} \tag{13}$$

where A_{ii} is the machinability attribute value, A_i is the original value, $A_{i\max}$ and $A_{i\min}$ are the maximum and minimum values of the original or recorded data, respectively.

According to the cutting theory, chip of type 1 can be given a value of 7, 3 for type 2.

As the attributes are influenced by each other, it is necessary to set a specified symbol, named relative importance, to show the mutual influence. The machinability evaluation is based on the calculation of the defined $n \times n$ machinability matrix as shown below.

$$B = \begin{bmatrix} A_{11} & a_{12} & a_{13} \\ a_{21} & A_{22} & a_{23} \\ a_{31} & a_{32} & A_{33} \end{bmatrix} \tag{14}$$

The diagonal values (i.e.,A_{ii}) represent the machinability attributes, and other items (i.e.,a_{ij}) represent the relative importance between the attributes. The relative importance a_{ij}, distributed the scale from 0 to 10, denotes the influence that an attribute i imposes on attribute j, while a_{ji} means the influence attribute j imposes on attribute i. a_{ij} and a_{ji} have the property:

$$a_{ij} + a_{ji} = 10 \tag{15}$$

This means that a scale is adopted from 0 to 10 on which the relative importance values are compared. This formula

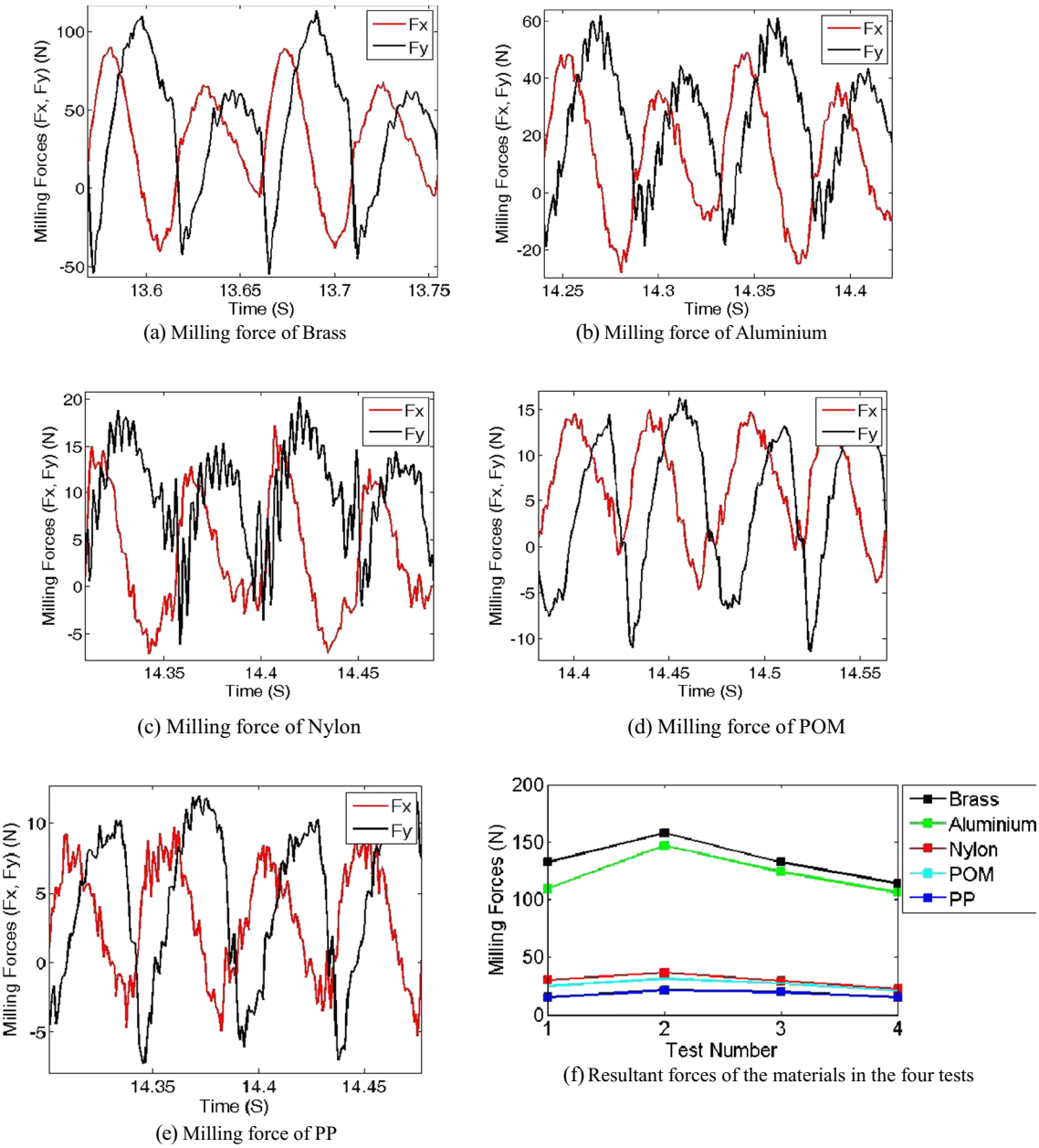

(a) Milling force of Brass
(b) Milling force of Aluminium
(c) Milling force of Nylon
(d) Milling force of POM
(e) Milling force of PP
(f) Resultant forces of the materials in the four tests

Fig. 7 Milling forces of the materials in test 1 and the resultant forces

gives an idea on the interaction between the machinability components as they are influenced mutually in practice, whereas the interactions were neglected in previous studies.

In order to reserve all of the information obtained from combinatorial consideration, permanent function is proposed [22], which is used in combinatorial mathematics [31]. The

Fig. 8 The "C" chip (type 1) (**a**, **b**) and the long, tight, and curly chips (type 2) (**c**–**e**)

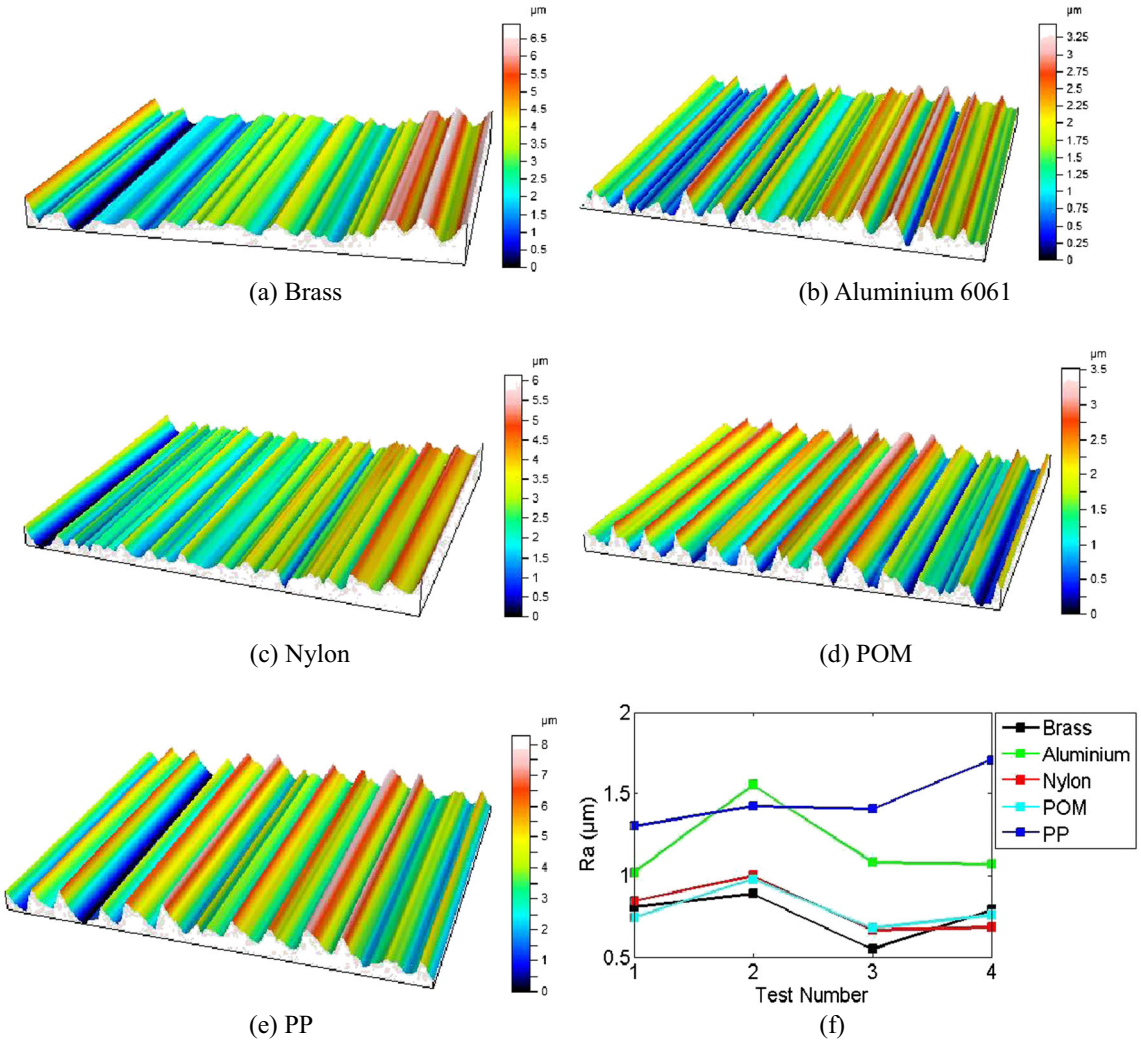

Fig. 9 Surface topography of the materials in test 1 (**a**–**e**) and the variation trend of surface roughness (**f**)

permanent function transforms negative signs in the determinant of the matrix to positive ones. This multinomial representation includes all the information regarding selected factors and ensures an estimate of the important factors affecting the machinability. It is a complete expression for the evaluation of machinability index as it considers presence of all factors and their interdependencies. Use of this concept in machinability evaluation will lead to a better appreciation of machinability attributes of the work materials. Thus, the higher the calculating result is, the better machinability the material possesses.

For the convenience of calculating the machinability matrix, label each material with a number as follows: brass-1, aluminum-2, nylon-3, POM-4, and PP-5. Table 6 shows the test results of machinability items of test 1. The values in Table 5 are converted according to the methodology described above and are given in Table 7.

To demonstrate the machinability matrix and calculation formula described above, taking brass, for example, the machinability matrix of test 1 is

$$B_{11} = \begin{bmatrix} 0 & 2 & 3 \\ 8 & 10 & 9 \\ 7 & 1 & 9 \end{bmatrix} \tag{16}$$

where subscripts i and j of B_{ij} represent the number of the test group and material, respectively. B_{11} is calculated in the following way:

$$\begin{aligned} p(B_{11}) &= 0 \times 10 \times 9 + 2 \times 9 \times 7 + 3 \times 1 \times 8 \\ &\quad + 3 \times 10 \times 7 + 9 \times 1 \times 0 + 9 \times 8 \times 2 \\ &= 504 \end{aligned} \tag{17}$$

Table 6 Test results

Material	Force (N)	Chip shape	Ra (μm)
1	132.3641	3	0.8051
2	109.1702	7	1.0192
3	24.8448	3	0.8410
4	29.9846	3	0.7445
5	15.0656	7	1.3019

Similarly, machinability index of test 1 for aluminum, nylon, POM, and PP are 248, 1,501, 1,289, and 240, respectively.

In Fig. 10, machinability indexes of the four tests are listed out according to the tests' results. Figure 10 shows that, for the same machining conditions, polyformaldehyde gets the highest machinability index followed by nylon and brass, which means that POM shows the best machinability among the five kinds of materials, and it is the appropriate material for manufacturing the MR-compatible robot. Brass gets higher machinability index than aluminum due to its smoother surface. Machinability indexes of aluminum and PP are similar. Nylon and POM gain obvious high indexes than other materials as cutting forces are lower and surfaces are smoother, while machinability index of PP is low as a result of its harsher surface and chip shape. However, the metals have low indexes largely due to the cutting forces compared with the engineering plastics.

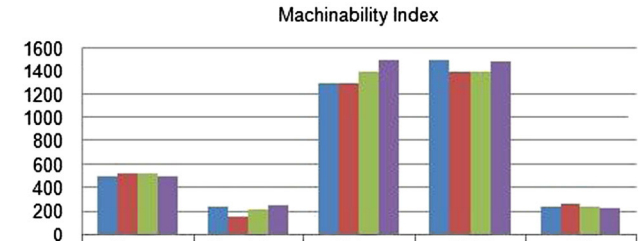

	Brass	Aluminium	Nylon	POM	PP
Test 1	504	248	1289	1501	240
Test 2	520	159	1289	1395	272
Test 3	520	223	1395	1395	240
Test 4	504	255	1501	1494	231

Fig. 10 Machinability index of the materials

4 Conclusions

In this paper, an improved mechanistic force model of flat-end milling is presented, and this paper makes a machinability evaluation of five kinds of candidate materials for MR-compatible robot. The main conclusions drawn in the present work can be summarized as below:

1. Mechanistic cutting force model is proposed. Tool runout and bottom-edge cutting effect are analyzed and incorporated into the model. The force coefficients are identified by applying a least squares fitting method. The proposed cutting force model is demonstrated to be effective. In addition, it is beneficial in further prediction of the necessary power, torque, vibrations, and reducing the cost.
2. Machinability evaluation for MR-compatible five materials is performed based on diagraph and matrix method. Brass is the best one in metals, and POM is verified to be the best in plastics. According to the diagraph and matrix method, POM gets the highest machinability value, which means it is the best candidate material among the tested materials for the MR-compatible robot.

Table 7 Machinability attribute values

Material	Force	Chip shape	Ra
1	0	10	9
2	2	0	5
3	9	10	8
4	9	10	10
5	10	0	0

Acknowledgments The authors would like to thank the National Natural Science Foundation of China (NSFC 51175373), Program for New Century Excellent Talents in University (NCET-10-0625), and Tianjin Key Laboratory of High Speed Cutting & Precision Machining (TUTE) (2013120024001167).

References

1. Dai J (2010) Surgical robotics and its development and progress. Robotica 28(3):161
2. Larson BT, Erdman AG, Tsekos NV, Yacoub E, Tsekos PV, Koutlas IG (2004) Design of an MRI-compatible robotic stereotactic device for minimally invasive interventions in the breast. J Biomech Eng-T ASME 126(4):458–465
3. Krieger A, Susil RC, Ménard C, Coleman JA, Fichtinger G, Atalar E, Whitcomb LL (2005) Design of a novel MRI compatible manipulator for image guided prostate interventions. IEEE Trans Biomed Eng 52(2):306–313
4. Chinzei K, Kikinis R, Jolesz FA (1999) MR compatibility of mechatronic devices: design criteria. In Proc. of MICCAI 1999 Conf. Cambridge, England, 1999: 1020–1030
5. Chinzei K, Hata N, Jolesz FA, Kikinis R (2000) MR compatible surgical assist robot: system integration and preliminary feasibility study. In Proc. of MICCAI 2000 Conf. Pittsburgh, 2000: 921–930
6. Stoianovici D (2005) Multi-imager compatible actuation principles in surgical robotics. Int J Med Robot Comput 1(2):86–100
7. Hu F, Li D (2012) Modelling and simulation of milling forces using an arbitrary Lagrangian–Eulerian finite element method and support vector regression. J Optim Theory Appl 153(2):461–484
8. Mounayri HEI, Badar MA, Rengifo GA (2008) Multi-parameter ANN model for flat-end milling. Trans Can Soc Mech Eng 32(3–4):523–536

9. Gonzalo O, Jauregi H, Uriarte LG, Lacalle LN (2009) Prediction of specific force coefficients from a FEM cutting model. Int J Adv Manuf Technol 43(3–4):348–356
10. Özel T, Altan T (2000) Process simulation using finite element method—prediction of cutting forces, tool stresses and temperatures in high speed flat end milling. Int J Mach Tools Manuf 40(5):713–738
11. Gradisek J, Kalveram M, Weinert K (2004) Mechanistic identification of specific force coefficients for a general end mill. Int J Mach Tools Manuf 44(4):401–414
12. Lamikiz A, Lacalle LN, Sánchez JA, Salgado MA (2004) Cutting force estimation in sculptured surface milling. Int J Mach Tools Manuf 44(14):1511–1526
13. Dang JW, Zhang WH, Yang Y, Wan M (2010) Cutting force modeling for flat end milling including bottom edge cutting effect. Int J Adv Manuf Technol 50(11):986–997
14. Ehmann KF, Kapoor SG, Devor RE, Lazoglu I (1997) Machining process modeling: a review. Trans ASME J Manuf Sci Eng 119(4B): 655–663
15. Oscar G, Jokin B, Haritz J (2010) A method for the identification of the specific force coefficients for mechanistic milling simulation. Int J Mach Tools Manuf 50(9):765–774
16. Roth D, Ismail F, Bedi S (2005) Mechanistic modelling of the milling process using complex tool geometry. Int J Adv Manuf Technol 25(1–2):140–144
17. Engin S, Altintas Y (2001) Mechanics and dynamics of general milling cutters. Part I: helical end mills. Int J Mach Tools Manuf 41(15):2195–2212
18. Rivière-Lorphèvre E, Filippi E (2009) Mechanistic cutting force model parameters evaluation in milling taking cutter radial runout into account. Int J Adv Manuf Technol 45(1–2):8–15
19. Kumar A, Choi SK, Goksel L (2011) Tolerance allocation of assemblies using fuzzy comprehensive evaluation and decision support process. Int J Adv Manuf Technol 55(1–4):379–391
20. Leon T, Liern V, Ruiz JL, Sirvent I (2003) A fuzzy mathematical programming approach to the assessment of efficiency with DEA models. Fuzzy Sets Syst 139(2):407–419
21. Rao RV, Gandhi OP (2002) Digraph and matrix methods for the machinability evaluation of work materials. Int J Mach Tools Manuf 42(3):321–330
22. Jangra K, Grover S, Chan FTS, Aggarwal A (2011) Digraph and matrix method to evaluate the machinability of tungsten carbide composite with wire EDM. Int J Adv Manuf Technol 56(9–12): 959–974
23. Lee B, Tarng Y, Li H (2000) An investigation of modeling of the machining database in turning operations. J Mater Process Technol 105(1–2):1–6
24. Li X, Hong W, Wang J, Song J, Kang J (2006) Research on the radar chart theory applied to the indoor environmental comfort level evaluation. In Proc. of WCICA 2006 Conf. Dalian, China, 2006: 5214–5217
25. Altintas Y (2000) Manufacturing automation. Cambridge University Press, Cambridge
26. Cifuentes ED, Garcia HP, Villasenor MG (2010) Dynamic analysis of runout correction in milling. Int J Mach Tools Manuf 50(8):709–717
27. Seethaler RJ, Yellowley I (1999) The identification of radial runout in milling operations. Trans ASME J Manuf Sci Eng 121(3):524–531
28. Karpat Y, Bahtiyar O, Deger B (2012) Mechanistic force modeling for milling of unidirectional carbon fiber reinforced polymer laminates. Int J Mach Tools Manuf 56:79–93
29. Budak E, Altintas Y, Armarego EJA (1996) Prediction of milling force coefficients from orthogonal cutting data. Trans ASME J Manuf Sci Eng 118(2):216–224
30. Irene BJ, Joan VC, Hernan GR (2011) Influence of feed, eccentricity and helix angle on topography obtained in side milling processes. Int J Mach Tools Manuf 51(12):889–897
31. Jurkat WB, Ryser HJ (1966) Matrix factorization of determinants and permanents. J Algebra 3:1–27